

## Article

# Static and Dynamic Analysis of 6-DOF Quasi-Zero-Stiffness Vibration Isolation Platform Based on Leaf Spring Structure

Zhen Wang <sup>1,2,3,\*</sup>, Chuanlin He <sup>1,2,3</sup>, Yan Xu <sup>1,2,3</sup>, Dong Li <sup>1,2,3</sup>, Zhanyuan Liang <sup>1,2,3</sup>, Wei Ding <sup>4</sup> and Lei Kou <sup>1,2</sup> 

<sup>1</sup> Institute of Oceanographic Instrumentation, Qilu University of Technology (Shandong Academy of Sciences), Qingdao 266318, China; hechuanlin@qlu.edu.cn (C.H.); xuyan@qlu.edu.cn (Y.X.); lidong19@qlu.edu.cn (D.L.); zhanyuan0733@qlu.edu.cn (Z.L.); koulei1991@qlu.edu.cn (L.K.)

<sup>2</sup> School of Ocean Technology Sciences, Qilu University of Technology (Shandong Academy of Sciences), Qingdao 266318, China

<sup>3</sup> Sino-Ukrainian Ocean Acoustics Technology Innovation Center, Qingdao 266318, China

<sup>4</sup> Shandong Provincial Key Laboratory of Computer Networks, Qilu University of Technology (Shandong Academy of Sciences), Jinan 250353, China; 701129@qlu.edu.cn

\* Correspondence: wangzqd@qlu.edu.cn

**Abstract:** Multi-degree-of-freedom isolator with low stiffness is a fair prospect in engineering application. In this paper, a novel 6-DOF QZS vibration isolation platform based on leaf spring structure is presented. Its bearing capacity is provided through four leaf springs, and the quasi-zero-stiffness is realized by the force balance between the central spring and the suspension spring. 6-DOF vibration isolation is realized by the ball-hinge fixed design of a leaf spring. Through static and dynamic analysis, the following conclusions are brought. The stiffness of the leaf spring and the deformation of the central spring under static load are directly proportional to the bearing capacity of the isolation table. Besides, in order to ensure that the stiffness of the system is close to zero, the stiffness of the suspension spring and the inner spring should be as similar as possible. The vertical and horizontal displacement transmissibility tests of the isolation platform are carried out, in which the jumping phenomenon in the QZS vibration isolation platform is analyzed. By improving the damping of the structure and the length of the suspension spring, the dynamic vibration isolation process of the system can be more stable, the transmissibility can be reduced, and the vibration isolation effect can be enhanced.

**Keywords:** vibration isolation platform; static and dynamic analysis; quasi-zero-stiffness; six degrees of freedom; transmissibility; nonlinear

**MSC:** 37G25



**Citation:** Wang, Z.; He, C.; Xu, Y.; Li, D.; Liang, Z.; Ding, W.; Kou, L. Static and Dynamic Analysis of 6-DOF Quasi-Zero-Stiffness Vibration Isolation Platform Based on Leaf Spring Structure. *Mathematics* **2022**, *10*, 1342. <https://doi.org/10.3390/math10081342>

Academic Editor: Ioannis G. Stratis

Received: 23 February 2022

Accepted: 8 April 2022

Published: 18 April 2022

**Publisher's Note:** MDPI stays neutral with regard to jurisdictional claims in published maps and institutional affiliations.



**Copyright:** © 2022 by the authors. Licensee MDPI, Basel, Switzerland. This article is an open access article distributed under the terms and conditions of the Creative Commons Attribution (CC BY) license (<https://creativecommons.org/licenses/by/4.0/>).

## 1. Introduction

Vibration isolator is regularly adopted to reduce or isolate the unexpected external disturbance on the normal running condition of precision equipment. In order to widen the load capacity, and increase the isolation efficiency, the ideal isolator is inclined to possess the higher static stiffness and lower dynamic stiffness, which is known as high-static and low-dynamic stiffness (HSLDS) [1].

Generally, the conventional isolators merely have the solo isolation component along the main vibration direction, such as the spring or rubber blanket. Nevertheless, it's difficult to fulfill the requirements of low frequency and large load-capacity simultaneously because of the linearity of the system stiffness. Since the early 1990s, quasi-zero-stiffness (QZS) vibration isolator with the characteristic of HSLDS has been proposed [2]. The main principle of QZS isolator is to realize the system stiffness near zero through adjustment of the components of positive and negative stiffness. Hence, QZS isolator can provide the higher load capacity, and comply with the essential requirements of subtle dynamic stiffness.

In the early decade, Alabuzhev [3] proposed several QZS isolator prototypes which included spring and buckled beam structure, single buckled beam structure, and ejector rod hinged joint with a spring structure. Whereafter, most of the QZS isolators are the improvements based on Alabuzhev's prototypes, and the main research concentrated on the realization of negative stiffness mechanism (NSM). Platus [4] designed the isolation structure with two rods hinged joint to each other to realize the NSM. Then, Liu et al. [5] adopted the Euler compression rods subjected to the axial preloading force as the NSM. Konvacic [6] used the symmetrically inclined spring and vertical spring to realize the QZS effect. The common disadvantage of the above structures is that the negative stiffness structure takes up more space. Therefore, Meng [7] later used leaf spring structure, and greatly reduced the volume of the vibration isolator. Carrella [8] combined the regular linear spring and permanent magnet in series to achieve QZS feature through equilibrating the elastic force and the magnetic force. Shin [9] carried out the engineering application based on Carrella's research. Shan [10] and Robertson [11] used the magnetic ring spring and permanent magnets structure, respectively, to achieve QZS. Besides, Araki [12] initiated the research from the functional materials. He proposed the superplastic Cu-Al-Mn shape memory alloy rod, which had the advantages of large load-capacity and stroke length. In recent years, more research transferred to the bionic structure area. Jing et al. [13,14] proposed the X-shaped and Z-shaped configurations on the basis of the leg structures of animals. Then, Gatti [15,16] proposed a K-shaped configuration consisting of four linear springs to increase the available vibration amplitude. Kim [17] presented the band-stop filter-type vibration isolator with V-shaped configuration inspired by the middle ear of the human auditory system. Although the above bio-inspired configurations are creative and possess the HSLDS characteristic, there is still the problem that the effective vibration displacement is difficult to meet the engineering application requirements.

For the reason that the actual excitations are in multiple directions and have the characteristics of low frequency and large amplitude, such as the wind load and wave load, the conventional QZS isolators are more difficult to achieve the better vibration isolation effect. Most existing solutions adopted the 6-DOF vibration isolator, and Stewart platforms with cubic or orthogonal structure are the most commonly used configurations from Wu et al. [18]. Zhou et al. [19] designed the QZS rod with cam-roller-spring structure as the NSM, and assembled a 6-DOF vibration isolation platform by combining the rods. Wang et al. [20] proposed the 6-DOF vibration isolation platform consisting of passive air springs and magnetostrictive actuators. Zhang et al. [21] proposed a hybrid vibration isolator composed of the active piezo stack actuator and the passive rubber isolator. Nevertheless, the complex adjustment is needed between each degree of freedom to achieve good vibration isolation effect. Hence, the active structures occupy most of the vibration isolators of this type. This is difficult to realize in the underwater environment where passive supplies are available.

From the above, the ideal isolator should maintain the quasi-zero dynamic stiffness and long-term stability over wide vibration amplitude [22]. Hence, it is practical to design a 6-DOF vibration isolation platform with the characteristics of compact structure, large load capacity, low natural frequency, and wide displacement range.

The main contributions of this paper are as follows:

- A novel 6-DOF QZS vibration isolation platform based on leaf spring structure is proposed, which consists of four leaf spring brackets for zero stiffness adjustment.
- Through the static analysis in different degrees of freedom, the effects of stiffness and dimension on the stiffness-displacement (rotation angle) relationship of the vibration isolation system are obtained.
- The influences of the damping and dimension parameters on the stability of the system were obtained through dynamic analysis. Moreover, the transmissibility characteristics were analyzed to evaluate the vibration isolation performance of the essential parameters determined in the static analysis and stability analysis. It is indicated that the system will tend to be more stable and there will be a better vibration

isolation effect when the damping and length parameters increase. Besides, the bifurcation of the isolation system will be caused as the amplitude of the excitation force increases, so that the vibration isolation effect will also decrease.

The remainder of this paper is organized as follows. The isolator structure is introduced, and the stiffness of the leaf spring is calculated in Section 2. Then, static analysis is carried out to obtain the relations of force- (or torque)-displacement (or angle) and stiffness-displacement (or angle) in Section 3. The dynamic analysis is proceeded to obtain the stability of the system response to external excitations in different degrees of freedom in Section 4. Moreover, the amplitude frequency response and the displacement transmissibility are compared to evaluate the parameter effects of damping and dimension. In order to verify the effect of vibration isolation, the vertical and horizontal displacement transmissibility tests of the isolation platform are given in Section 5. Finally, the conclusions and future recommendations are contained in Section 6.

## 2. Structural Description

There are several common disadvantages in the existing 6-DOF QZS vibration isolation platform, which are the large volume, complicated adjustment, and narrow displacement range. Therefore, a novel 6-DOF QZS vibration isolation platform based on leaf spring structure is presented.

### 2.1. Structure and Mechanism

The platform mainly consists of top plate, base plate, spring bracket, and central spring. The top plate is used to fix vibration-isolated objects, and the base plate is the fixed surface of the whole platform. The spring bracket is placed between the top and base plates, and rotates symmetrically around the vertical axis of the base plate at an angular interval of  $90^\circ$ . The central spring is fixed along the centerline of the top and base plates by hanging rings. The schematic of the platform is shown in Figure 1.

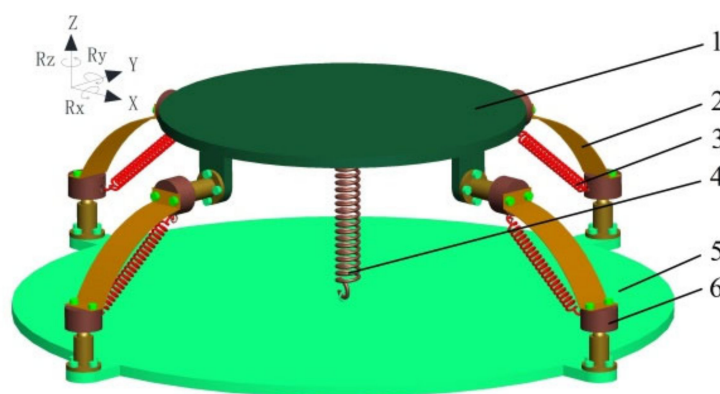


**Figure 1.** Schematic of the platform: (1) top plate; (2) leaf spring; (3) suspension spring; (4) central spring; (5) base plate; (6) spherical hinge.

The leaf spring and suspension spring are fixed to the spherical hinge by bolt and hanged ring connection, respectively. These two springs are used to coordinate with the central spring for system stiffness adjustment. Since the leaf springs are blocked in the lateral direction, the relative rotation between the top and base plates is achieved through a spherical hinge in which the leaf spring can rotate around the fixed point.

The system stiffness is adjusted by the spring bracket and the central spring. In the initial state, the central spring is stretched and provides negative stiffness. The leaf springs and suspension springs are compressed and provide positive stiffness. The loaded weight is supported by the leaf spring, and hence, the selection of leaf spring should satisfy the load capacity requirement. As to the system stiffness in different degree of freedom, the stretch or compression state of each spring will change with the stiffness adjustment.

2.2. Stiffness Analysis of Leaf Spring

In order to calculate the stiffness, the leaf spring is approximately equivalent to the cantilever, as shown in Figure 2.

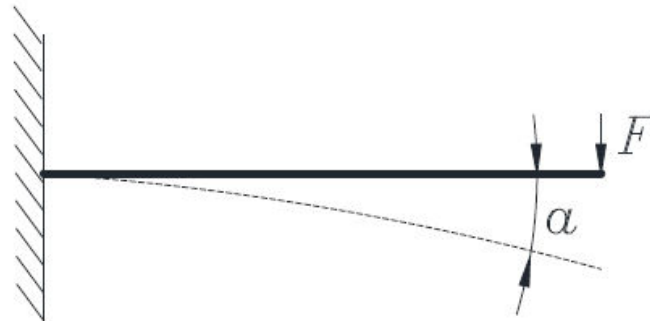


Figure 2. Schematic diagram of leaf spring force analysis.

The force-bearing end of the leaf spring rotates  $\alpha$  under the force  $F$ , and the moment of inertia can be defined as Equation (1):

$$J = \frac{1}{12}bh^3 \tag{1}$$

where  $b$  is the width of leaf spring, and  $h$  is the thickness.

Under the load force  $F$ , the angle  $\alpha$  can be obtained by Mohr’s theorem, which is defined as Equation (2):

$$\alpha = \int_0^l \frac{F \cdot x \cdot dx}{E \cdot J} = \int_0^l \frac{12F \cdot x \cdot dx}{E \cdot b \cdot h^3} = \frac{6Fl^2}{E \cdot b \cdot h^3} \tag{2}$$

where  $l$  is the length of leaf spring and  $E$  is elasticity modulus.

The dimension of the leaf spring is shown in Figure 3.

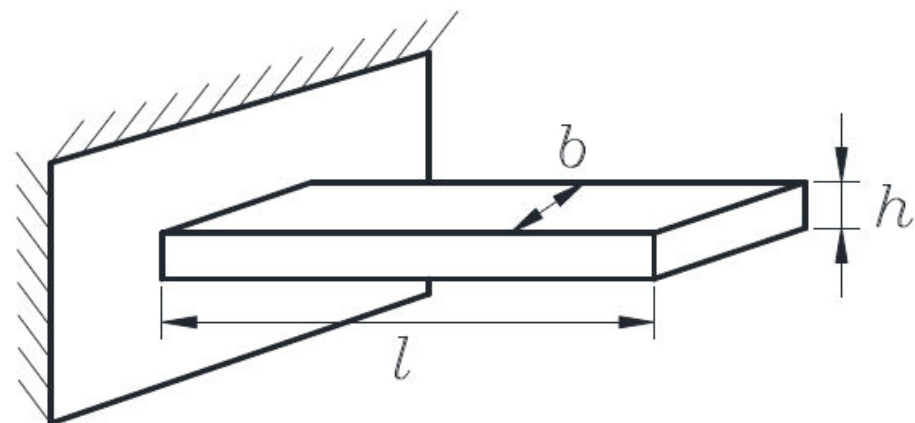


Figure 3. Dimensions of leaf spring.

Hence, the force  $F$  can be calculated as Equation (3):

$$F = \frac{E \cdot b \cdot h^3}{6 \cdot l^2} \cdot \alpha \tag{3}$$

As to the stiffness of suspension spring, the force condition is shown in Figure 4.

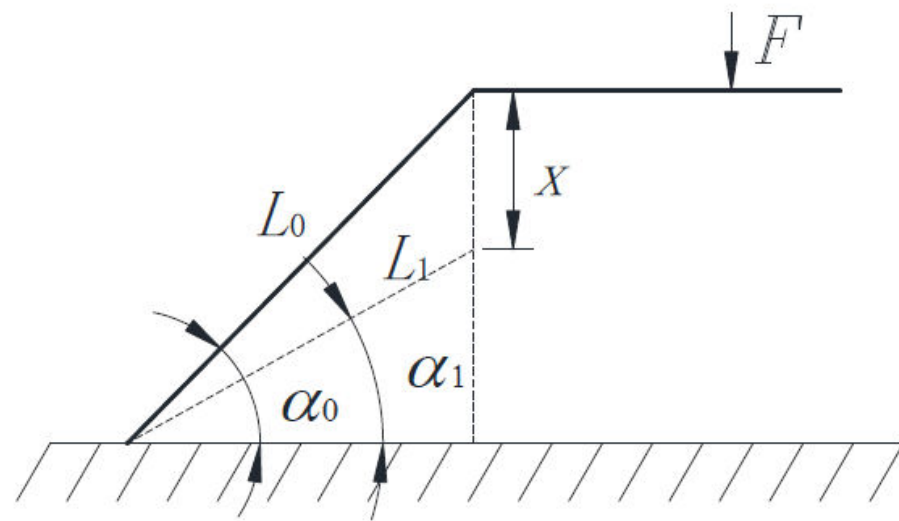


Figure 4. Schematic diagram of suspension spring force analysis.

As shown in Figure 4, the parameters of  $L_0, \alpha_0$  are the initial length and slant angle of suspension spring, respectively.  $x$  is the displacement of top plate under the force  $F$ . Then, the relation of force and displacement is calculated as Equation (4):

$$\begin{cases} F = k_1 \cdot (L_0 - L_1) \\ x = L_0 \cdot \sin \alpha_0 - L_1 \cdot \sin \alpha_1 \end{cases} \quad (4)$$

### 3. Static Analysis

#### 3.1. Establishment of Statics Model

Since the platform is axisymmetric structure, the different degree of freedom is classified into vertical displacement, horizontal displacement, vertical rotation, and horizontal rotation.

##### 3.1.1. Vertical Displacement

The static loading status of the platform in vertical displacement is shown in Figure 5. There is the downward displacement  $x_1$  in the top plate under the vertical force  $F_{vd}$  from the initial state  $I_v$  to the second state  $II_v$ . Accordingly, the length of suspension spring decreases from  $L_{20}$  to  $L_{2v}$ , and the slant angle changes from  $\alpha$  to  $\beta$ , and the leaf spring has a rotation angle of  $\theta_v$ . Besides, the central spring has the initial stretch length of  $L_1$ . In the state  $II_v$ , the central spring is still stretched, whereas the suspension spring and leaf spring are both compressed. Hence, the positive stiffness is provided by the leaf spring and suspension spring, and the negative stiffness is provided by central spring.

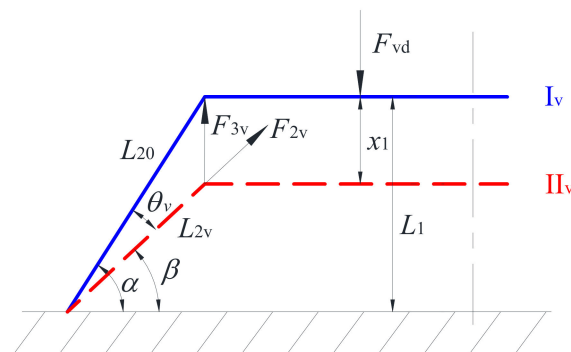


Figure 5. Schematic diagram of vertical displacement.

According to the force balance in vertical direction, the relation of the vertical force  $F_{vd}$ , elastic force of suspension spring  $F_{2v}$  and elastic force of leaf spring  $F_{3v}$  can be calculated as Equation (5):

$$F_{vd} + k_1 \cdot (L_1 - x_1 - L_{10}) = F_{2v} \cdot \sin \beta + F_{3v} \tag{5}$$

where  $k_1$  is the stiffness of central spring, and  $L_{10}$  is unstretched length of the central spring.

In order to obtain the value of  $F_{vd}$  from Equation (3), the rotation angle of the leaf spring needs be calculated firstly. From Figure 5, there are the relations of  $\alpha$  and  $\beta$  that  $\sin \alpha = L_1/L_{20}$ ,  $\sin \beta = (L_1 - x_1)/L_{2v}$ ,  $\cos \alpha = \sqrt{L_{20}^2 - L_1^2}/L_{20}$ ,  $\cos \beta = \sqrt{L_{20}^2 - L_1^2}/L_{2v}$ .

In the case where the rotation angle of leaf spring is small enough, the approximation of  $\theta_v \approx \sin \theta_v = \sin(\alpha - \beta)$ , then  $\theta_v$  can be calculated as Equation (6):

$$\theta_v = \frac{x_1 \cdot \sqrt{L_{20}^2 - L_1^2}}{L_{20} \cdot L_{2v}} \tag{6}$$

Substituting Equations (3) and (6) into Equation (5) yields Equation (7):

$$F_{vd} = \frac{k_2 \cdot L_{20}}{L_{2v}} \cdot (L_1 - x_1) - (k_1 + k_2) \cdot (L_1 - x_1) + \frac{E \cdot b \cdot h^3 \cdot x_1}{6L_{2v} \cdot L_{20}^3} \cdot \sqrt{L_{20}^2 - L_1^2} + k_1 \cdot L_{10} \tag{7}$$

where  $k_2$  is the stiffness of suspension spring. By introducing the non-dimensional parameters  $\hat{F}_{vd} = F_{vd}/k_1 \cdot L_{20}$ ,  $\hat{x}_1 = (x_1 - L_1)/L_{20}$ ,  $\hat{k}_3 = E \cdot b \cdot h^3 / (6k_1 \cdot L_{20}^3)$ ,  $A = k_2/k_1$ ,  $\hat{L}_1 = L_1/L_{20}$ ,  $\hat{L}_{2v} = \sqrt{\hat{x}_1^2 + 1 - \hat{L}_1^2}$ , and the term of  $L_{10}/L_{20}$  can be eliminated, since the value of  $L_{10}$  is small enough relative to  $L_{20}$ , thus the non-dimensional form of Equation (7) can be rewritten as Equation (8):

$$\hat{F}_{vd} = \hat{x}_1 + A \cdot \hat{x}_1 \cdot \left(1 - \frac{1}{\hat{L}_{2v}}\right) + \hat{k}_3 \cdot \frac{\sqrt{1 - \hat{L}_1^2}}{\hat{L}_{2v}} \cdot (\hat{x}_1 + \hat{L}_1) \tag{8}$$

Hence, the non-dimensional stiffness of vertical displacement can be obtained by differentiating  $\hat{F}_{vd}$  with respect to  $\hat{x}_1$  as Equation (9):

$$\hat{K}_{vd} = \frac{\partial \hat{F}_{vd}}{\partial \hat{x}_1} = 1 + A + \frac{-A \cdot (1 - \hat{L}_1^2) + \hat{k}_3 \cdot \sqrt{1 - \hat{L}_1^2} \cdot (1 - \hat{L}_1 + \hat{x}_1 \cdot \hat{L}_1)}{(\hat{x}_1^2 + 1 - \hat{L}_1^2)^{\frac{3}{2}}} \tag{9}$$

### 3.1.2. Horizontal Displacement

The force condition in horizontal displacement analysis is shown in Figure 6. The top plate has a leftward displacement  $x_2$  under the horizontal force  $F_{hd}$  from the initial state  $I_h$  to the second state  $II_h$ . Therefore, the length of the left and right springs will change inconsistently. The length of suspension spring decreases from  $L_{20}$  to  $L_{2h1}$  in the left, and increases from  $L_{20}$  to  $L_{2h2}$  in the right, and both sides of the leaf springs have a same rotation angle of  $\theta_h$ . Moreover, the central spring also rotates  $\theta_h$  from its initial position. In the state  $II_v$ , the central spring is stretched, whereas the suspension springs are both compressed. Although the leaf springs are also compressed, the horizontal force is offset by the interaction of the left and right leaf springs. Hence, the positive stiffness is provided by leaf spring and left suspension spring, and the negative stiffness is provided by right suspension spring.

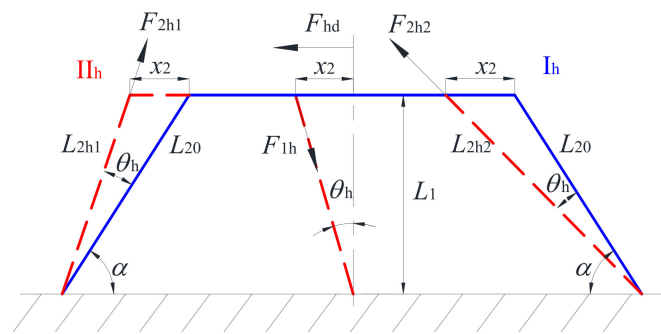


Figure 6. Schematic diagram of horizontal displacement.

The relation of the horizontal force  $F_{hd}$ , and the elastic force of suspension spring  $F_{2h1}$  and  $F_{2h2}$  can be calculated as Equation (10):

$$F_{hd} + F_{2h2} \cdot \cos(\alpha - \theta_h) = F_{2h1} \cdot \cos(\alpha + \theta_h) + F_{1h} \cdot \sin \theta_h \tag{10}$$

According to the relations of rotation angles and dimensions in Figure 6, there are  $\cos(\alpha - \theta_h) = \sqrt{L_{2h2}^2 - L_1^2} / L_{2h2}$ ,  $\sin \theta_h = x_2 / \sqrt{x_2^2 + L_1^2}$ ,  $\cos(\alpha + \theta_h) = \sqrt{L_{2h1}^2 - L_1^2} / L_{2h1}$ . By introducing the non-dimensional parameters  $\hat{F}_{vh} = F_{vh} / k_1 \cdot L_{20}$ ,  $\hat{x}_2 = x_2 / L_{20}$ ,  $\hat{L}_{2h1} = \sqrt{(\sqrt{1 - \hat{L}_1^2 - \hat{x}_2^2})^2 + \hat{L}_1^2}$ ,  $\hat{L}_{2h2} = \sqrt{(\sqrt{1 - \hat{L}_1^2 + \hat{x}_2^2})^2 + \hat{L}_1^2}$ , the non-dimensional form of Equation (10) can be expressed as Equation (11):

$$\hat{F}_{hd} = A \cdot \left( \frac{1}{\hat{L}_{2h1}} + \frac{1}{\hat{L}_{2h2}} \right) - 2 \cdot \sqrt{1 - \hat{L}_1^2} + \left( 1 - \frac{\hat{L}_1}{\sqrt{\hat{x}_2^2 + \hat{L}_1^2}} - A \cdot \left( \frac{1}{\hat{L}_{2h1}} - \frac{1}{\hat{L}_{2h2}} \right) \right) \cdot \hat{x}_2 \tag{11}$$

### 3.1.3. Vertical Rotation

The force condition in vertical rotation analysis is shown in Figure 7. The top plate has a contrarotation under the torque  $M_{vm}$  around the vertical axis, and hence, there is the rotation angle  $\theta_{vm}$  from the initial state  $I_{vm}$  to the second state  $II_{vm}$ . Moreover, the length of suspension spring increases from  $L_{20}$  to  $L_{2vm}$ , and the slant angle changes  $\theta_{vm}$  horizontally and circumferentially, and the leaf spring has a rotation angle of  $\theta_{vm1}$ . Besides, there is no change in the central spring. In the state  $II_v$ , the suspension spring and leaf spring are both compressed, whereas the positive stiffness is provided by the leaf spring, and the negative stiffness is provided by the suspension spring because the direction of torque on the two springs is different.

The relation of the torque  $M_{vm}$ , elastic force of the suspension spring  $F_{2vm}$ , and elastic force of the leaf spring  $F_{3vm}$  can be calculated as Equation (12):

$$M_{vm} + F_{2vm} \cdot \sin \theta_{vm1} \cdot L_0 = F_{3vm} \cdot \cos \theta_{vm1} \cdot L_0 \tag{12}$$

where  $L_0$  is the radius of top plate.

According to the relations of rotation angle and radius in Figure 7, there are  $\sin \theta_{vm1} = L_0 \cdot \theta_{vm} / \sqrt{L_0^2 \cdot \theta_{vm}^2 + L_{20}^2}$ ,  $\cos \theta_{vm1} = L_{20} / \sqrt{L_0^2 \cdot \theta_{vm}^2 + L_{20}^2}$ ,  $\theta_{vm1} \approx \sin \theta_{vm1}$ . By introducing the non-dimensional parameter  $\hat{M}_{vm} = M_{vm} / (k_1 \cdot L_{20} \cdot L_0)$ , the non-dimensional form of Equation (12) can be expressed as Equation (13):

$$\hat{M}_{vm} = -A \cdot \frac{\theta_{vm} \cdot \hat{L}_0}{\sqrt{(\theta_{vm} \cdot \hat{L}_0)^2 + 1}} \cdot (\sqrt{(\hat{L}_0 \cdot \theta_{vm})^2 + 1} - 1) + \hat{k}_3 \cdot \frac{\hat{L}_0 \cdot \theta_{vm}}{(\hat{L}_0 \cdot \theta_{vm})^2 + 1} \tag{13}$$

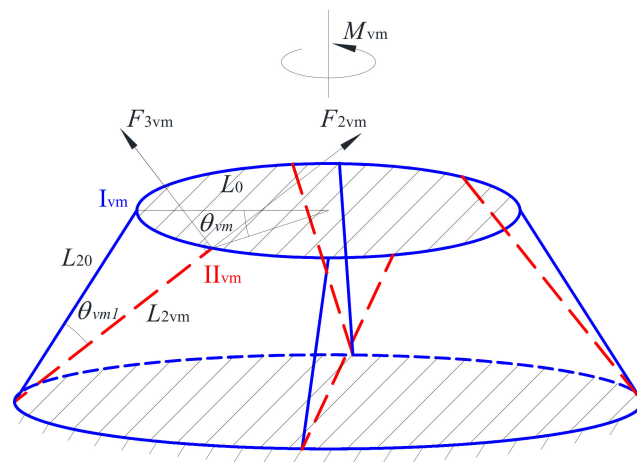


Figure 7. Schematic diagram of vertical rotation.

### 3.1.4. Horizontal Rotation

The force condition in horizontal rotation analysis is shown in Figure 8. The top plate has a contrarotation under the torque  $M_{hm}$  around the horizontal axis, and hence, there is the rotation angle  $\theta_{hm}$  from the initial state  $I_{hm}$  to the second state  $II_{hm}$ . Moreover, the length of the left and right springs will change inconsistently. The length of the suspension spring decreases from  $L_{20}$  to  $L_{2hm1}$  in the left, and increases from  $L_{20}$  to  $L_{2hm2}$  in the right, and both sides of the leaf springs have the same rotation angle of  $\theta_{hm}$ . Besides, there is no change in the central spring. In the state  $II_v$ , the suspension spring and leaf spring are both compressed, whereas the positive stiffness is provided by the leaf spring and suspension spring in the left, and the negative stiffness is provided by the leaf spring and suspension spring in the right because the direction of torque on the two springs is different.

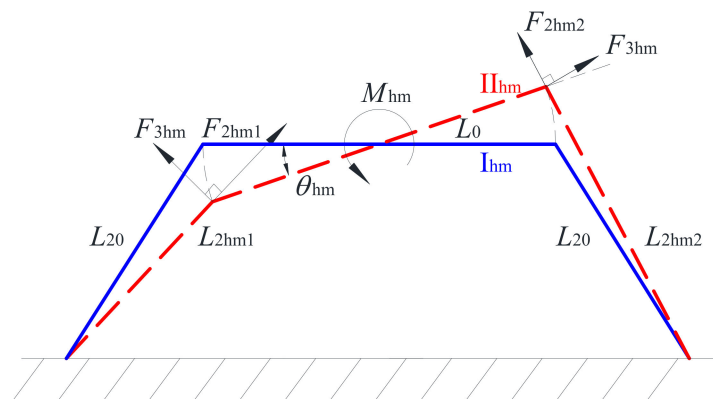


Figure 8. Schematic diagram of horizontal rotation.

The relation of the torque  $M_{hm}$ , elastic force of the suspension spring  $F_{2hm1}$  and  $F_{2hm2}$ , elastic force of the leaf spring  $F_{3hm}$  can be calculated as Equation (14):

$$M_{hm} + F_{2hm2} \cdot \cos \theta_{hm} \cdot L_0 + F_{3hm} \cdot \sin \theta_{hm} \cdot L_0 = F_{2hm1} \cdot \sin \theta_{hm} \cdot L_0 + F_{3hm} \cdot \cos \theta_{hm} \cdot L_0 \quad (14)$$

Similarly, if the rotation angle of the leaf spring is small enough, there is the approximation of  $\theta_{hm} \approx \sin \theta_{hm}$ ,  $L_{2hm1} \approx L_{20} - \theta_{hm} \cdot L_0 \cdot \cos \theta_{hm}$ ,  $L_{2hm2} \approx L_{20} + \theta_{hm} \cdot L_0 \cdot \cos \theta_{hm}$ . By introducing the non-dimensional parameters  $\hat{M}_{hm} = M_{hm} / (k_1 \cdot L_{20} \cdot L_0)$ , the non-dimensional form of Equation (14) can be expressed as Equation (15):

$$\hat{M}_{hm} = (A \cdot \hat{L}_0 \cdot \sqrt{1 - \theta_{hm}^2} - \hat{k}_3) \cdot \theta_{hm} \cdot (\theta_{hm} - \sqrt{1 - \theta_{hm}^2}) \quad (15)$$

### 3.2. Relations of Force (Torque), Stiffness, and Displacement (Rotation Angle)

The essential condition that the QZS vibration isolation system can be realized is that the system stiffness at the static equilibrium position should be zero. Hence, there are some premises in the different degrees of freedom related to the parameters of dimension and stiffness.

#### 3.2.1. Vertical Displacement

According to Equation (9), there is the premise that the condition of  $\hat{K}_{vd}(\hat{x}_1 = 0) = 0$  can be fulfilled and expressed as Equation (16):

$$1 + A - \frac{A}{\sqrt{1 - \hat{L}_1^2}} + \hat{k}_3 = 0 \tag{16}$$

On account of  $\hat{k}_3 > 0$ , then Equation (16) can be defined as Equation (17):

$$A > \frac{1}{(1 - \hat{L}_1^2)^{-\frac{1}{2}} - 1} \tag{17}$$

#### 3.2.2. Horizontal Displacement

According to Equation (11), when  $\hat{x}_2 = 0$ ,  $\hat{K}_{hd}$  is always zero.

#### 3.2.3. Vertical Rotation

According to Equation (13), the premise that the condition of  $\hat{K}_{vm}(\theta_{vm} = 0) = 0$  can be fulfilled is expressed as Equation (18):

$$\hat{k}_3 \cdot \hat{L}_0 = 0 \tag{18}$$

#### 3.2.4. Horizontal Rotation

According to Equation (15), the premise that the condition of  $\hat{K}_{hm}(\theta_{hm} = 0) = 0$  can be fulfilled is expressed as Equation (19):

$$\hat{k}_3 = A \cdot \hat{L}_0 \tag{19}$$

In conclusion, there are two constraint conditions for stiffness  $A$ ,  $\hat{k}_3$  and dimensions  $\hat{L}_1, \hat{L}_0$  in all other three degrees of freedom, except horizontal displacement, as follows.

Deduced by Equation (19), one of the parameters  $\hat{k}_3$  and  $\hat{L}_0$  must be zero, whereas it is impossible in reality. In other words, the system stiffness merely achieves quasi-zero value in vertical displacement. Consequently, if the value of  $\hat{K}_{vm}$  is expected to be less, then,  $\hat{k}_3$  or  $\hat{L}_0$  needs to be reduced as low as possible.

During the determination of stiffness and dimension parameters, the value of  $\hat{L}_1$  should be evaluated at first. Then the ranges of  $\hat{k}_3, A, \hat{L}_0$  are delimited according to Equations (16), (17), and (19). Finally, the values of  $A, \hat{k}_3, \hat{L}_1, \hat{L}_0$  are analyzed by the comparison of force-displacement curves, and the precondition of the system stiffness at the static equilibrium position needs to be zero.

In the following analysis, the value of  $\hat{L}_1$  is predetermined as  $\sqrt{3}/2$ , which means that the angle between the lower end of the suspension spring and the base plate is  $60^\circ$ . Hence,

the result of  $A > 1$  can be determined by Equation (17), and then, the values of  $A$  are defined as 1.1, 1.5, 2. Moreover, the values of  $\hat{k}_3$  are defined as 0.1, 0.5, 1 by Equation (16), and the values of  $\hat{L}_0$  are defined as 0.1, 0.3, 0.5 by Equation (19). With the parameters setting above, the variations of stiffness to displacement are shown in Figure 9.

As shown in Figure 9, the stiffness value will be close to zero when the value of  $A$  is close to 1. Hence, the effective variation ranges of the displacement (rotation angle) will be wider. Besides, it is shown in Figure 9b that the stiffness value of the vertical rotation at the static equilibrium position is close to zero, not equal to zero, which belongs to the quasi-zero stiffness state, whereas the system stiffness of the other degrees of freedom are all zero.

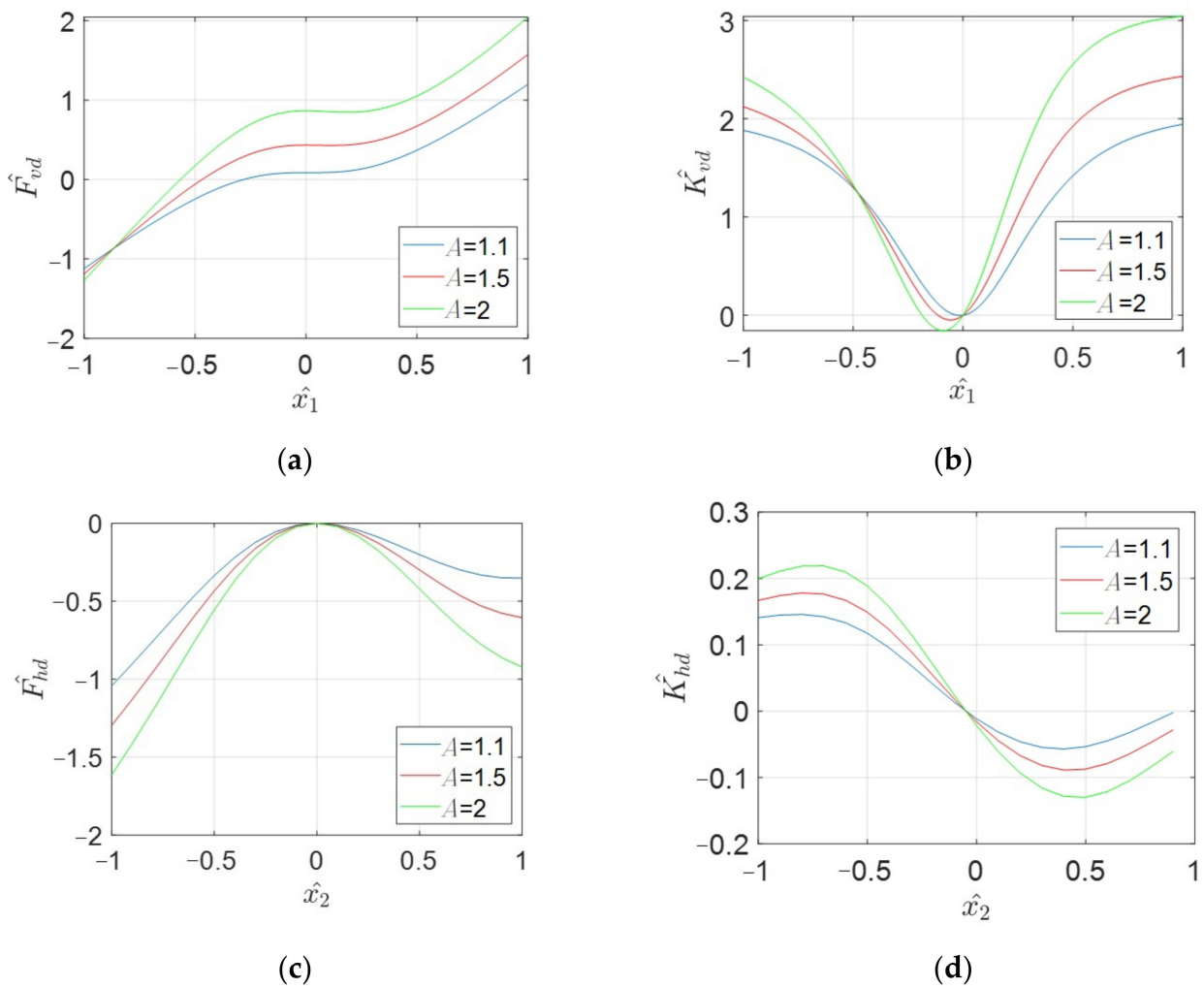
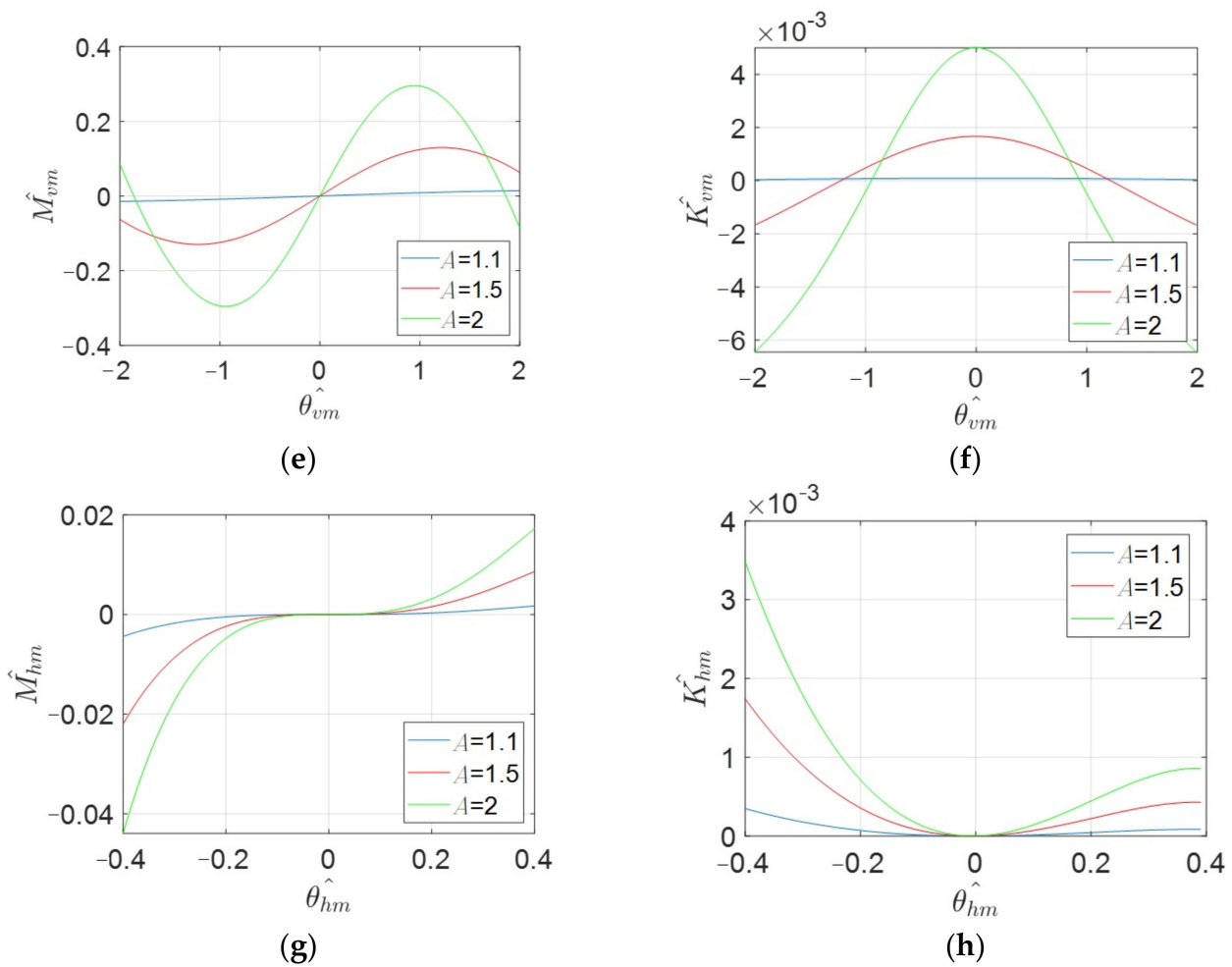


Figure 9. Cont.



**Figure 9.** Variations of stiffness with displacement: (a) force in vertical displacement; (b) force in horizontal displacement; (c) force in vertical rotation; (d) force in horizontal rotation; (e) stiffness in vertical displacement; (f) stiffness in horizontal displacement; (g) stiffness in vertical rotation; (h) stiffness in horizontal rotation.

Based on the analysis result, the non-dimensional values are  $A = 1.1$ ,  $\hat{k}_3 = 0.1$ ,  $\hat{L}_1 = \sqrt{3}/2$ ,  $\hat{L}_0 = 0.1$ .

In addition, there are cubic relations between force and displacement from Figure 9. Therefore, the approximate expressions of the force can be expanded with the third order Taylor series near the static equilibrium position, and rewritten as Equations (20)–(23):

$$\hat{F}_{vd}(\hat{x}_1) = \hat{F}_{vd}(0) + \hat{F}'_{vd}(0) \cdot \hat{x}_1 + \frac{\hat{F}''_{vd}(0)}{2!} \cdot \hat{x}_1^2 + \frac{\hat{F}'''_{vd}(0)}{3!} \cdot \hat{x}_1^3 = \left(\frac{A}{2a^3} - \frac{\hat{k}_3}{2a^2}\right) \cdot \hat{x}_1^3 - \frac{b}{2a^2} \cdot \hat{x}_1^2 + \left(A + 1 - \frac{A}{a} + k_3\right) \cdot \hat{x}_1 + b \quad (20)$$

$$\hat{F}_{hd}(\hat{x}_2) = (-3A \cdot a + 3A \cdot a^3) \cdot \hat{x}_2^2 + \frac{1}{2L_1} \cdot \hat{x}_2^3 \quad (21)$$

$$\hat{M}_{vm} = \hat{k}_3 \cdot \hat{L}_0 \cdot \theta_{vm} - \left(\frac{A \cdot \hat{L}_0^3}{2} + \hat{k}_3 \cdot \hat{L}_0\right) \cdot \theta_{vm}^3 \quad (22)$$

$$\hat{M}_{hm} = (A \cdot \hat{L}_0 - \hat{k}_3) \cdot (-\theta_{hm} + \theta_{hm}^2 + \frac{1}{2} \theta_{hm}^3) \quad (23)$$

The maximum difference is no more than 3.5%, and is near to zero in the vertical rotation.

Another essential design parameter is the static load capacity. In order to realize the requirement of the static load force  $G$  being completely supported by four leaf springs, the tensile force  $F_1$  provided by the central spring and the elastic force  $F_2$  provided by the suspension springs should be balanced out to be zero.

In order to illustrate the approximate deviation, comparisons between Equations (20)–(23) and Equations (8), (11), (13), and (15) are shown in Figure 10.

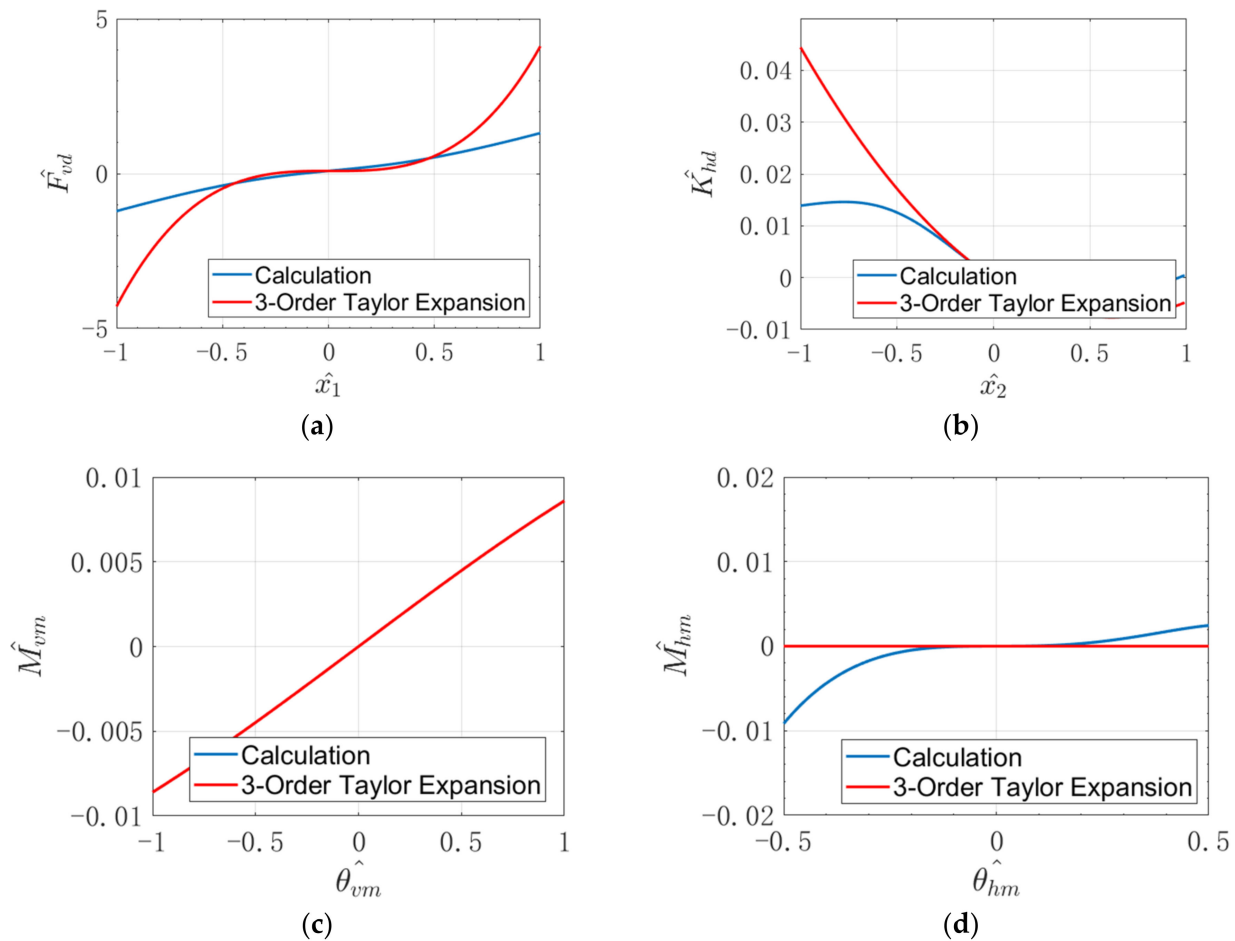


**Figure 10.** Comparisons of force-displacement curves: (a) vertical displacement; (b) horizontal displacement; (c) vertical rotation; (d) horizontal rotation.

It is indicated in Figure 10 that the variation tendency of  $\hat{F}_{vd}$ ,  $\hat{F}_{hd}$ ,  $\hat{M}_{vm}$ , and  $\hat{M}_{hm}$  can be approximated using the third-order Taylor series within a small deviation near the static equilibrium position. The maximum difference is no more than 3.5%, and is near to zero in the vertical rotation.

Another essential design parameter is the static load capacity. In Figure 11, the initial load condition of the QZS vibration isolator is illustrated. In order to realize the requirement of the static load force  $G$  being completely supported by four leaf springs, the tensile force,  $F_1$ , provided by the central spring and the elastic force,  $F_2$ , provided by the suspension springs should be balanced out to be zero.

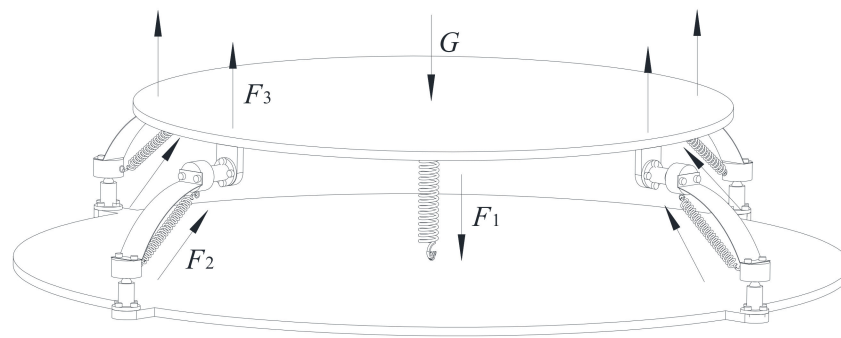


Figure 11. Schematic diagram of initial load condition.

Deduced by Equation (21), the static load force  $G$  is mainly related to parameters  $\hat{k}_3$ ,  $\hat{L}_1$ ,  $\hat{x}_0$ , and expressed as Equation (24):

$$\hat{G} = \hat{k}_3 \cdot \theta = \hat{k}_3 \cdot \frac{\hat{x}_0 \cdot \sqrt{1 - \hat{L}_1^2}}{\sqrt{\hat{x}_0^2 + 1 - \hat{L}_1^2}} \tag{24}$$

where  $\hat{x}_0$  is the vertical displacement of the isolator when it only bears the static load force.

Based on the values of  $\hat{k}_3$  and  $\hat{L}_1$  already determined, the variation of  $\hat{G}$  with  $\hat{x}_0$  is shown in Figure 12.

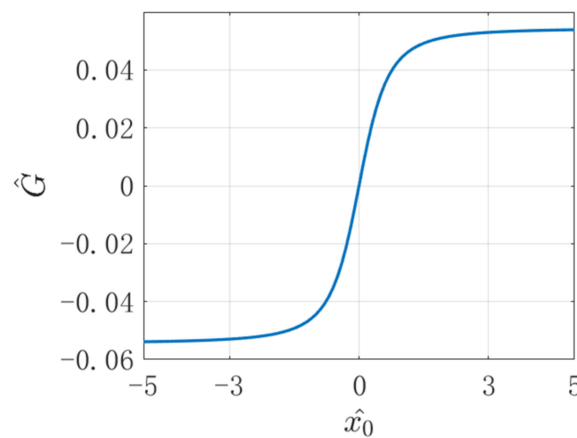


Figure 12. Variation of  $\hat{G}$  with  $\hat{x}_0$ .

It can be clearly noted from Figure 12. that  $\hat{G}$  starts out proportional to  $\hat{x}_0$ , and then it stays constant when the absolute value of  $\hat{x}_0$  is greater than 3. This indicates that the load capacity of the platform is proportional to the initial displacement of the top plate. Moreover, there is also high relevancy between  $\hat{G}$  and  $\hat{k}_3$  from Equation (24), whereas  $\hat{G}$  changes less with  $\hat{L}_1$ . The reason is that  $\hat{L}_1$  is related to static equilibrium position; hence, there is a similar variation tendency of  $\hat{G}$  with  $\hat{x}_0$  whether  $\hat{L}_1$  increases or decrease under the premise of Equation (17). Conclusively, the load capacity of the isolator is mainly related to the stiffness of the leaf spring and the deformation of the central spring under static load.

### 4. Dynamic Analysis

#### 4.1. Establishment of Dynamic Models

The influence of damping parameters is taken into account in the dynamics models. The responses and the external excitations are expressed as Equation (25):

$$\begin{cases} \mathbf{u} = \{u_1, u_2, u_3, u_4\} \\ \mathbf{v} = \{v_1, v_2, v_3, v_4\} = \{H_1 \sin \omega t, H_2 \sin \omega t, H_3 \sin \omega t, H_4 \sin \omega t\} \end{cases} \tag{25}$$

Consequently, the dynamics models are established as Equation (26):

$$\mathbf{M} \times \ddot{\mathbf{u}} = -\mathbf{C} \times (\dot{\mathbf{u}} - \dot{\mathbf{v}}) - \mathbf{F}_k \tag{26}$$

where the mass matrix is  $\mathbf{M} = \{m, m, I_{vm}, I_{hm}\}$ , the damping matrix is  $\mathbf{C} = \{C_1, C_2, C_3, C_4\}$ , and the force matrix is  $\mathbf{F}_k = \{F_{vd}, F_{hd}, M_{vm}, M_{hm}\}$ .

According to Equations (20)–(23), and introducing the non-dimensional parameters  $\Omega = \omega/\omega_0, \tau = \omega_0 \cdot t, \omega_0 = \sqrt{k_1/M_i}, \zeta_i = C_i \cdot \omega_0/2k_1, \hat{H}_{1,2} = H_{1,2}/L_{20}, \hat{H}_{3,4} = H_{3,4}/L_{20}, \hat{f}_i = \hat{H}_i \cdot \Omega^2$ , Equation (26) can be rewritten as Equation (27):

$$\begin{cases} \ddot{\hat{w}}_1 + 2\zeta_1 \dot{\hat{w}}_1 + \left( d_1 \cdot \hat{w}_1^3 + d_2 \cdot \hat{w}_1^2 + d_3 \cdot \hat{w}_1 + b \right) = \hat{f}_1 \cdot \sin \Omega \tau \\ \ddot{\hat{w}}_2 + 2\zeta_2 \dot{\hat{w}}_2 + \left( d_4 \cdot \hat{w}_2^2 + d_5 \cdot \hat{w}_2^3 \right) = \hat{f}_2 \cdot \sin \Omega \tau \\ \ddot{\hat{w}}_3 + 2\zeta_3 \dot{\hat{w}}_3 + \left( d_6 \cdot \hat{w}_3 + d_7 \cdot \hat{w}_3^3 \right) = \hat{f}_3 \cdot \sin \Omega \tau \\ \ddot{\hat{w}}_4 + 2\zeta_4 \dot{\hat{w}}_4 + \left( d_8 \cdot (-\hat{w}_4 + \hat{w}_4^2 + \frac{1}{2} \hat{w}_4^3) \right) = \hat{f}_4 \cdot \sin \Omega \tau \end{cases} \tag{27}$$

where  $d_1 = A/2a^3 - k_3/2a^2, d_2 = -b/2a^2, d_3 = A + 1 - A/a + k_3, d_4 = -3A \cdot a + 3A \cdot a^3, d_5 = 1/2L_1, d_6 = k_3 \cdot L_0, d_7 = -A \cdot L_0/2 - k_3 \cdot L_0, d_8 = A \cdot L_0 - k_3$ .

For the quantitative analysis, the harmonic balance (HB) method is applied, and the fundamental response is assumed to be Equation (28):

$$\hat{w}_i(\tau) = \hat{w}_i\left(\tau + \frac{2\pi}{\Omega}\right) = \hat{W}_i \cdot \sin(\Omega\tau + \theta_i) \tag{28}$$

where  $\theta_i$  and  $\hat{W}_i$  are, respectively, the phase and amplitude of the response.

During the approximate process, the higher order harmonic terms of  $\cos 2\Omega\tau, \sin 3\Omega\tau$ , and  $\cos 3\Omega\tau$  are neglected.

Substituting Equation (28) into Equation (27) results in Equation (29):

$$\begin{cases} \left( \frac{3}{4} \cdot d_1 \right)^2 \cdot \hat{W}_1^6 + \left( \frac{3}{2} \cdot d_1 \right) \cdot (d_3 - \Omega^2) \cdot \hat{W}_1^4 + ((d_3 - \Omega^2)^2 + (2\Omega \cdot \zeta_1)^2) \cdot \hat{W}_1^2 - \hat{f}_1^2 = 0 \\ \left( \frac{3}{4} \cdot d_5 \right)^2 \cdot \hat{W}_2^6 - \left( \frac{3}{2} \cdot d_5 \cdot \Omega^2 \right) \cdot \hat{W}_2^4 + (\Omega^4 + (2\Omega \cdot \zeta_2)^2) \cdot \hat{W}_2^2 - \hat{f}_2^2 = 0 \\ \left( \frac{3}{4} \cdot d_7 \right)^2 \cdot \hat{W}_3^6 + \left( \frac{3}{2} \cdot d_7 \right) \cdot (d_6 - \Omega^2) \cdot \hat{W}_3^4 + ((d_6 - \Omega^2)^2 + (2\Omega \cdot \zeta_3)^2) \cdot \hat{W}_3^2 - \hat{f}_3^2 = 0 \\ \left( \frac{3}{8} \cdot d_8 \right)^2 \cdot \hat{W}_4^6 - \left( \frac{3}{4} \cdot d_8 \right) \cdot (d_8 + \Omega^2) \cdot \hat{W}_4^4 + ((d_8 + \Omega^2)^2 + (2\Omega \cdot \zeta_4)^2) \cdot \hat{W}_4^2 - \hat{f}_4^2 = 0 \end{cases} \tag{29}$$

#### 4.2. Stable Analysis

In order to carry out the stable analysis, the parameters are determined based on the vibration isolation of large instruments. According to the conclusion in Figure 12, the value of  $\hat{G}$  will be less than 0.05, then there is  $\hat{G} \leq 0.05$ . The value of  $L_{20}$  is chosen as less than

1 depending on the size of the platform. For the reason that the bearing capacity of the platform is no less than 50 kg, the value of  $k_1$  is calculated by Equation (24):

$$m = \frac{G}{g} = \frac{\hat{G} \cdot k_1 \cdot L_{20}}{g} \geq 50\text{kg} \tag{30}$$

Hence, the parameters are set to  $k_1 = 2 \times 10^4\text{N/m}$ ,  $m = 50\text{ kg}$ .

The influences of the parameters of damping ratio  $\zeta_i$  and slant length  $L_{20}$  are analyzed. On account of the material of the platform mainly being steel, the variant range of damping ratio  $\zeta_i$  is 0.0158~0.158, which means the deformation of the structure is within the elastic range. The excitation parameter  $\hat{H}_i$  is set to 0.6, which means the largest excitation amplitude will be 0.6 m.

During the bifurcation analysis, the time step is 0.001 of a period  $T$ , and the absolute error is  $10^{-6}$ . The excitation frequency is 6.28 rad/s. To eliminate the effects of transient response, only the data from the last 400 periods are plotted in the diagrams.

#### 4.2.1. Damping

The global bifurcation variations with the damping ratio are shown in Figure 13.

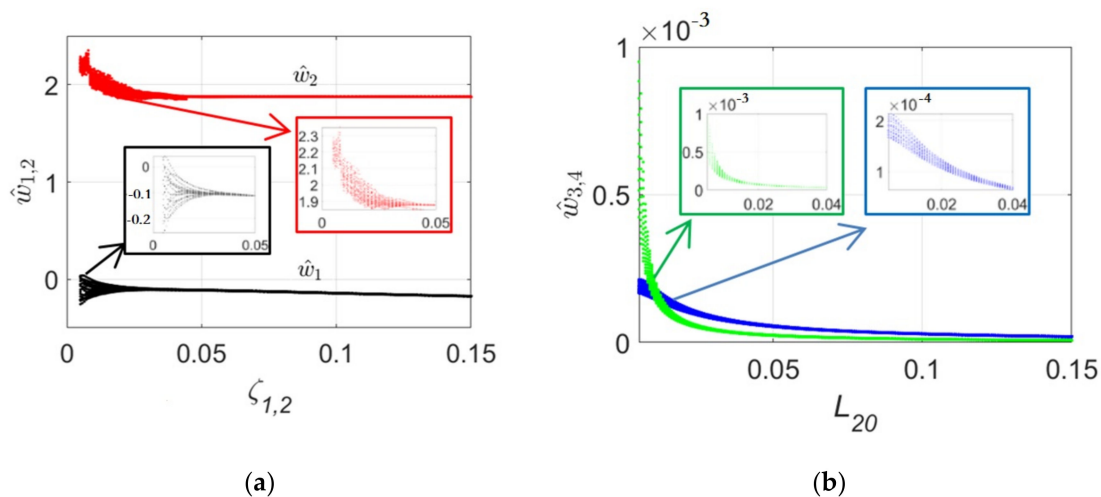


**Figure 13.** Bifurcation diagram of the displacement and rotation responses for varying  $\zeta_i$ : (a) displacement; (b) rotation. Black and blue line are vertical, red and green line are horizontal.

It is shown in Figure 13 that the displacement responses tend to be stable as the damping increases, and exhibit steady-state periodical motion in the range of  $\zeta_i > 0.06$ . Moreover, the effect of damping on the displacement is more obvious by comparing the displacement and rotation response. Especially in the range of  $\zeta_i < 0.05$ , the chaos occurs in the displacement responses, and weak in the rotation responses. In addition, it seems that the vertical responses in both displacement and rotation take less time to stabilize. Besides, the response amplitude will decrease as the damping increases.

#### 4.2.2. Slant Length

The variation of global bifurcation with length parameters is illustrated in Figure 14.

It is shown in Figure 14a that the displacement response tends to be stable when  $L_{20}$  is greater than 0.2, and the value is constant. The vertical response magnitude is larger than the horizontal response. There is chaos occurring in the range of  $L_{20} < 0.2$ . In Figure 14b, the rotation response will gradually decrease, and the period number will increase when the slant length increases, especially in horizontal response. The reason for that is the compressing length of the leaf spring and suspension spring will decrease, whereas there is not any variant in the central spring. Therefore, the total stiffness of the platform will be

unbalanced, and then, the response will become correspondingly unstable. Consequently, increasing the slant length will improve the vibration isolation effect, nevertheless the unstable response will also be introduced.

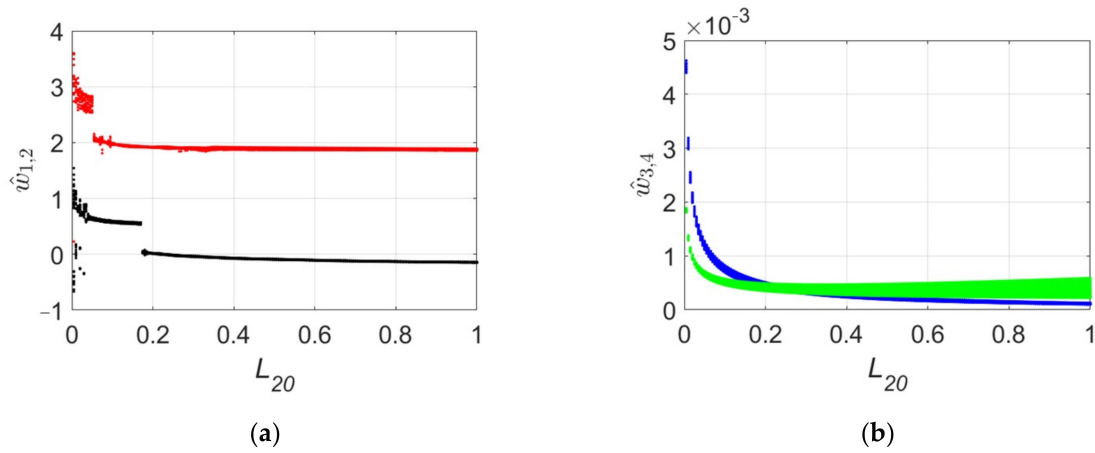


**Figure 14.** Bifurcation diagrams of the displacement and rotation responses for varying  $L_{20}$ : (a) displacement; (b) rotation. Black and blue line are vertical, red and green line are horizontal.

4.2.3. Periodical Analysis

The results above show that the displacement responses are periodic, except some chaotic variations which are induced by the QZS adjustment. Hence, the periodical analysis needs to be carried out to determine the influence of design parameters on the system stability. The parameters are set as  $\zeta_i = 0.07$ ,  $\hat{H}_{1,2} = 0.6$ ,  $\hat{H}_{3,4} = 5^\circ$ ,  $L_{20} = 0.6$ , and the results are demonstrated in Figures 15–18.

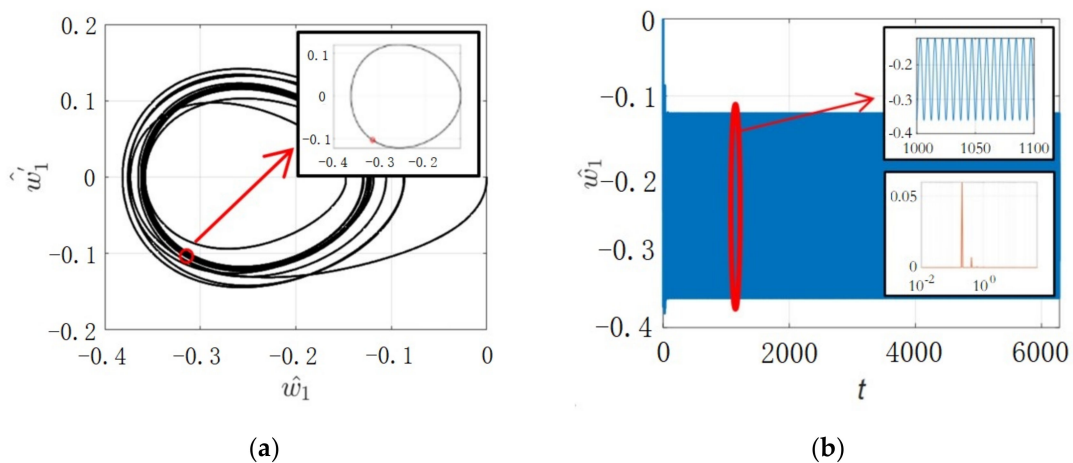


**Figure 15.** Periodical analysis of vertical displacement: (a) Poincaré phase diagram; (b) time history.

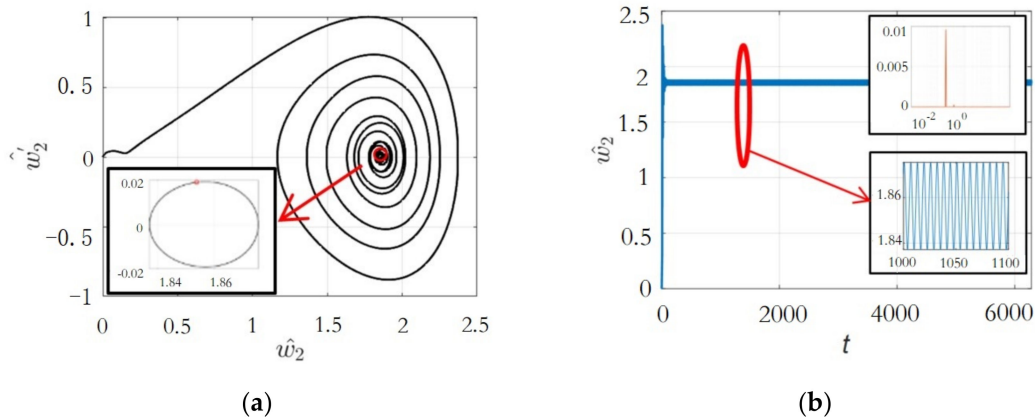


Figure 16. Periodical analysis of horizontal displacement: (a) Poincaré phase diagram; (b) time history.

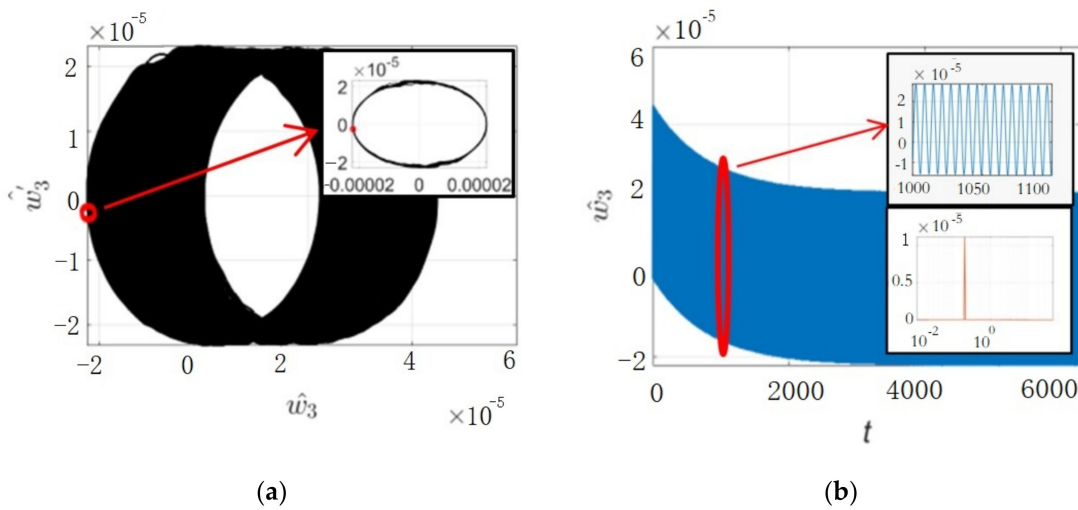


Figure 17. Periodical analysis of vertical rotation: (a) Poincaré phase diagram; (b) time history.

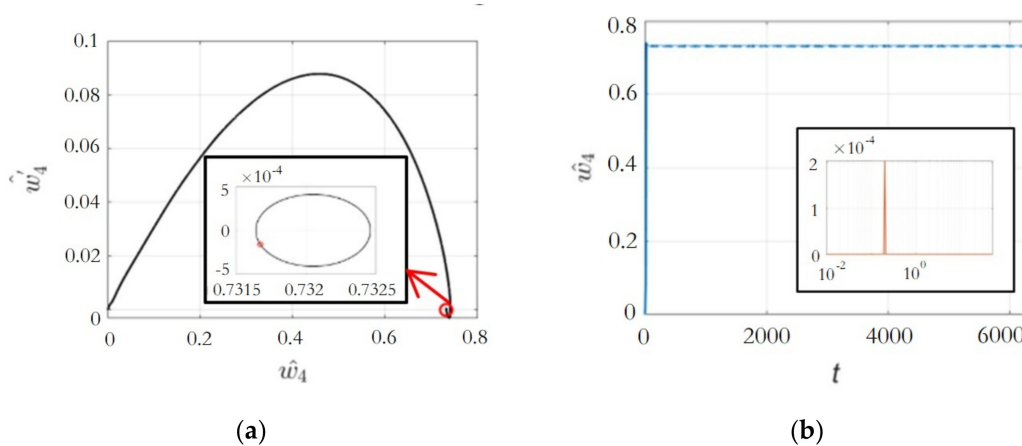


Figure 18. Periodical analysis of horizontal rotation: (a) Poincaré phase diagram; (b) time history.

It is shown in Figures 15–18 that the response in each degree of freedom will have a large amplitude of transient response in the beginning, and then eventually oscillate in the form of single-period steady-state vibration. All the vibration responses are dominated by the excitation frequency. Hence, the chaotic motion occurs only for a very short time at the beginning of the isolation operation. In conclusion, the vibration displacement response

of the vibration isolation platform in each degree of freedom will be steady-state periodic vibration eventually.

4.3. Characteristics of Transmissibility

The displacement transmissibility is adapted here, which is obtained by Equation (25) as Equation (31):

$$T_i = \frac{|\hat{u}_i|}{|\hat{v}_i|} = \frac{|\hat{v}_i + \hat{w}_i|}{|\hat{v}_i|} \tag{31}$$

where  $\hat{v}_i = \hat{H}_i \sin \omega t$ ,  $\hat{w}_i = \hat{W}_i \cdot \sin(\Omega\tau + \theta_i)$ .

Then, Equation (31) is rewritten as Equation (32):

$$T_i = \frac{\sqrt{\hat{W}_i^2 + \hat{H}_i^2 + 2\hat{W}_i \cdot \hat{H}_i \cdot \cos \theta_i}}{\hat{H}_i} \tag{32}$$

4.3.1. Damping

According to Section 4.2, the value of damping  $\zeta_i$  is set as 0.0158, 0.07, and 0.158. The comparison results are shown in Figure 19.

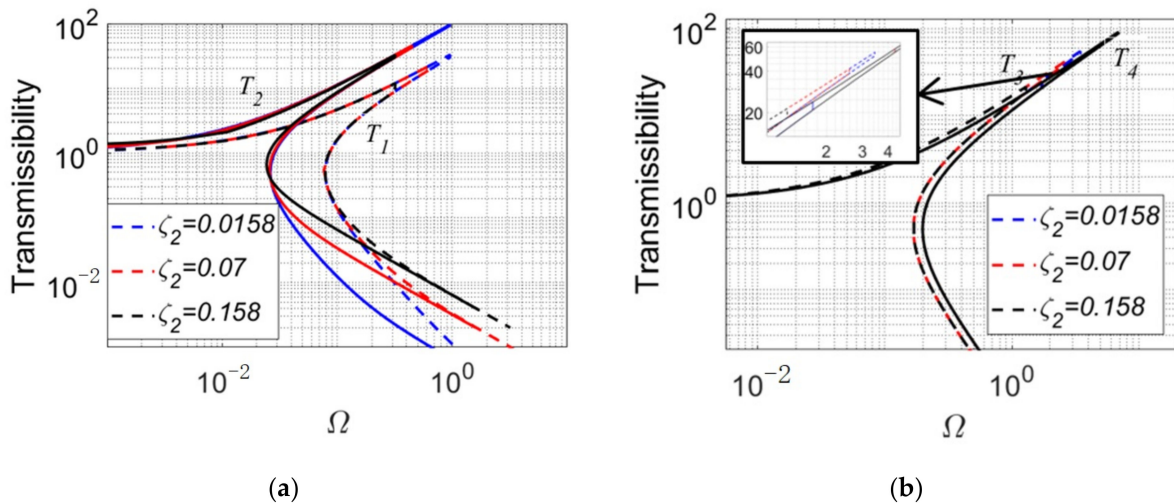


Figure 19. Comparison of displacement transmissibility in variation with damping: (a) displacement; (b) rotation. Dash lines show the vertical results, solid lines show the horizontal results.

The following conclusions can be drawn from Figure 19.

Increasing the damping will reduce the peak value of the system in the resonance region, which is more obvious in the displacement transmissibility. When the damping parameter is large enough, the frequency jump phenomenon will disappear, and the linear amplitude-frequency variation will be generated.

When there is  $T_i \geq 1$ , increasing the damping will reduce the transmissibility, which is shown in Figure 19a. On the contrary, when there is  $T_i < 1$ , which means the excitation frequency is greater than the system resonance frequency, the transmissibility will increase with the damping.

Through the comparison of vertical and horizontal transmissibility, there is a more obvious difference in the displacement. The reason for the small difference in rotation is that the effect of the central spring is smaller than that of the other springs.

### 4.3.2. Slant Length

The value of slant length  $L_{20}$  is set as 0.1, 0.6, and 1. The comparison results are shown in Figure 20.

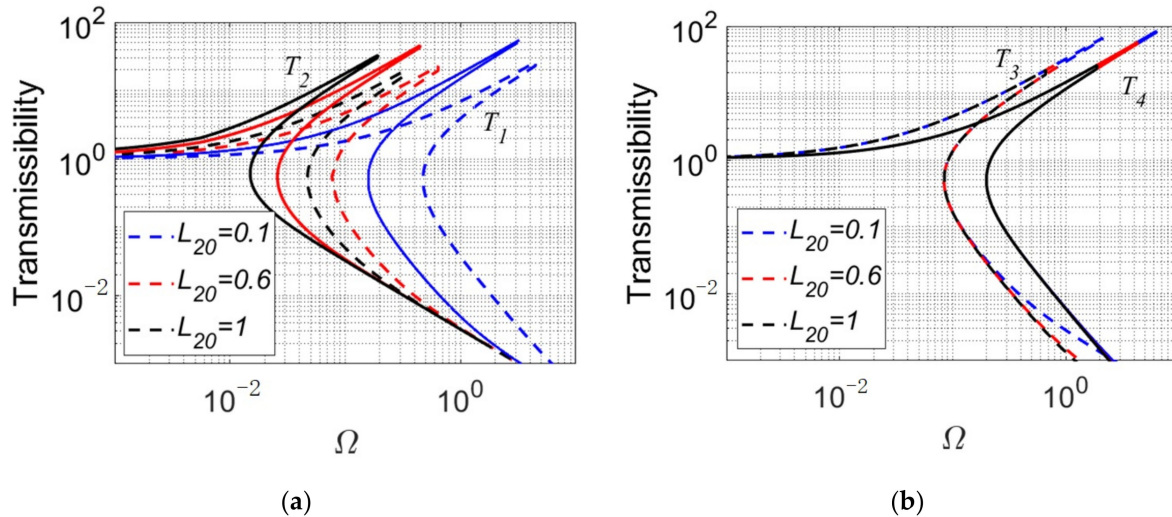


**Figure 20.** Comparison of displacement transmissibility in variation with slant length: (a) displacement; (b) rotation. Dash lines show the vertical results, solid lines show the horizontal results.

It is illustrated from Figure 20a that the resonance peak values and the initial vibration isolation frequencies in the displacement will gradually decrease with the increase of the slant length. The reason for the above phenomenon is that the increase of the slant length will reduce the rigidity of the suspension spring, so it will reduce the rigidity of the entire system. Nevertheless, only the resonance peak decreases with the increase of the length in the rotation variable, which also explains the same phenomenon as the third conclusion in Section 4.3.1.

## 5. Experimental Investigation

### 5.1. Experimental Instrument Setup

In order to verify and analyze the effect of vibration isolation, a set of 6-dOF quasi-zero stiffness vibration isolation platform is built in this paper, and the stiffness and dimension parameters are based on the results of Sections 3 and 4. The parameters of the isolation table are listed in Table 1.

**Table 1.** The physical parameters for building the experimental platform.

| Parameters                          | Symbol   | Value      |
|-------------------------------------|----------|------------|
| Stiffness of central spring         | $k_1$    | 20,000 N/m |
| Stiffness of suspension spring      | $k_2$    | 22,000 N/m |
| Stiffness of leaf spring            | $k_3$    | 2000 N/m   |
| Initial length of central spring    | $L_1$    | 0.52 m     |
| Initial length of suspension spring | $L_{20}$ | 0.6 m      |
| Radius of top plate                 | $L_0$    | 0.06 m     |
| Damping                             | $C_i$    | 44.3 N·m   |
| Excitation amplitude                | $H_i$    | 0.1 m      |
| Static load                         | $m$      | 50 kg      |

In addition, the material of each component of the vibration isolation table is shown in Table 2.

**Table 2.** The material parameters.

| Components            | Material        |
|-----------------------|-----------------|
| Central spring        | Stainless steel |
| Suspension spring     | Stainless steel |
| Leaf spring           | Mn-steel        |
| Top and base plates   | Stainless steel |
| Spherical hinge       | Stainless steel |
| Screws and fastenings | Stainless steel |

The central spring and the suspension spring of the vibration isolation platform are all selected as a round section cylindrical spring, in which the vertical spring is used as a stretch spring, and the oblique spring is used as a compression spring. The spring parameters can be selected according to Equation (33) and the size parameters in Table 1.

$$k_i = \frac{Gd^4}{8nD^3} \tag{33}$$

where  $d$  is the wire diameter of spring,  $D$  is the middle diameter of spring,  $n$  is the number of turns, and  $G$  is the shear modulus of material.

According to Table 2, the material shear modulus of spring is  $G = 79,380 \text{ N/mm}^2$ , and the parameters of the central spring and the suspension spring can be calculated according to Equation (33), which are listed in Table 3.

**Table 3.** The physical parameters of the springs.

| Type              | $d$ -mm | $D$ -mm | $n$ | $L$ -mm | $k$ -N/m |
|-------------------|---------|---------|-----|---------|----------|
| Central spring    | 10      | 60      | 23  | 465     | 19,973   |
| Suspension spring | 8       | 35      | 42  | 607     | 22,570   |

The size of the leaf spring can be selected according to Equation (3) and parameter  $L_{20}$ , and finally determined as:  $b = 80 \text{ mm}$ ,  $h = 2 \text{ mm}$ . The shape of the whole vibration isolation platform and the configuration of the measurement system are shown in Figure 21.

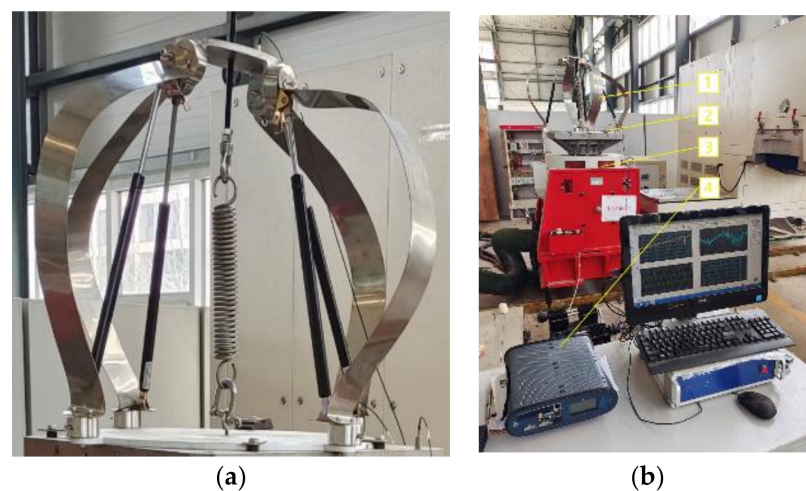


**Figure 21.** Six degrees of freedom quasi-zero stiffness vibration isolation platform and its test setup: (a) the experiment platform; (b) test on site ((1) 6-DOF QZS platform; (2) accelerometer; (3) vibrator; (4) acquisition instrument).

The horizontal and vertical vibration excitation tests of the isolation platform were carried out. The response values of input and output terminals of the isolation platform were measured by the accelerometers fixed on the base and the top surface of the platform, and the displacement transmissibility was compared and analyzed. During the experiment, the linear vibration isolation performance is achieved by removing the central spring and four suspension springs on the vibration isolation platform, and only by four leaf springs. The instrument configuration of the whole measurement system is shown in Table 4.

Table 4. Experimental instrument setup.

| Instruments             | Models              | Parameters   |
|-------------------------|---------------------|--|
| Vibration table         | ACT2000-R0225S, CMI | Max. Force: 22 kN, Max. Acceleration: 1000 m/s <sup>2</sup> ,<br>Frequency Range: 1~3000 Hz. |
| Accelerometer           | 4529-B, B&K         | Sensitivity: 10 mV/ms <sup>-2</sup> , Frequency range: 0.3~6.0 kHz,<br>Weight: 14.5 g.       |
| Data Acquisition System | CRONOS-PL-3, imc    | 16 channels, Max. sampling rate: 400 kS/s  |

5.2. Experiment Analysis

Due to the experimental conditions, this verification test mainly analyzes the displacement transmissibility of vertical and horizontal displacement degrees of freedom. According to the correlation of vibration reduction performance of the platform in terms of translational and rotational degrees of freedom mentioned above, the experimental results can also provide preliminary guiding significance for vibration reduction under rotational excitation.

The forward and reverse linear frequency sweep excitation is used in the experiment. The frequency range of the excitation force is 0.5–20 Hz, the sweep duration is 60 s, and the frequency interval is 0.32 Hz.

The vertical and horizontal displacement transmissibility obtained by the test is compared in Figure 22.

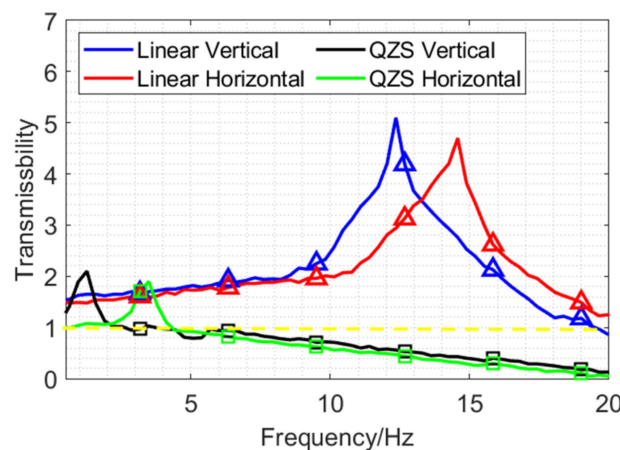


Figure 22. Experimental comparison of vertical and horizontal displacement transmissibility between the linear system and the quasi-zero-stiffness.

As can be seen from Figure 22, when the platform is in linear mode, its initial vibration isolation frequency is about 19.32 Hz in vertical vibration, and larger than 20 Hz in horizontal vibration. In the quasi-zero stiffness mode, the initial vibration isolation frequency is about 2.22 Hz (vertical) and 4.43 Hz (horizontal), which is about 10 Hz lower than that in the linear mode.

According to the platform parameters given in Table 1, the natural frequency of the platform can be calculated from Equation (27) as 20 Hz. In addition, combined with

the theoretical calculation results of transmissibility in Figures 19 and 20, it can be seen that the effective initial vibration isolation frequency of the platform is 0.1~0.2 times the natural frequency: about 2~4 Hz. Therefore, the above test results are basically in line with the expectation of theoretical calculation. At the same time, the vibration isolation frequency of vertical displacement is about 2 Hz smaller than that of horizontal displacement, about 0.1 times the natural frequency, which is also consistent with the characteristics of Figures 19 and 20. This indicates that compared with the corresponding linear isolation platform, the QZS vibration isolation platform expands the vibration isolation range, reduces the initial vibration isolation frequency, and has a great possibility to achieve low-frequency vibration isolation, which is basically consistent with theoretical research.

In addition, in order to verify the frequency jump phenomenon of the QZS vibration isolation system, the reverse frequency sweep experiment was carried out on the premise of keeping the experimental settings unchanged. The forward and reverse displacement transmissibility are compared in Figure 23.

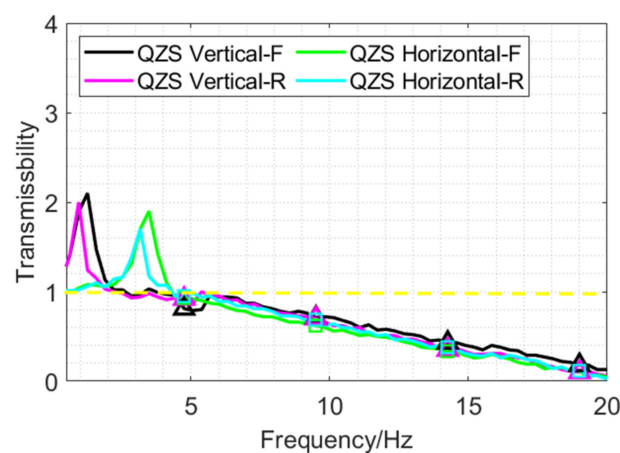


**Figure 23.** Comparison of forward and reverse frequency sweep displacement transmissibility of QZS system.

As shown in Figure 23, in the case of forward frequency sweeping, the initial vibration isolation frequency of the vibration isolation platform is about 2.22 Hz (vertical) and 4.43 Hz (horizontal). In reverse frequency sweep, the initial vibration isolation frequencies are 1.90 Hz (vertical) and 4.12 Hz (horizontal), respectively. This indicates that the QZS vibration isolation platform has a jumping phenomenon, and its jump-down frequency is 2.22 Hz (vertical) and 4.43 Hz (horizontal), and its jump-up frequency is 1.90 Hz (vertical) and 4.12 Hz (horizontal), resulting in a jumping interval of 0.32 Hz (vertical) and 0.31 Hz (horizontal). Therefore, it can be verified through the experiment that the cause of the jump phenomenon is caused by the inconsistency between the jump frequency and the jump frequency generated in the forward and reverse frequency sweep.

At the same time, there will be damping differences caused by different degrees of lubrication and tightness in the connection of components of the platform itself, which will also affect the vibration isolation frequency differences in the process of forward and reverse frequency sweeping. Therefore, it is necessary to study the change of vibration isolation effect caused by contact friction damping in the future, and put forward a standardized process for the manufacture and installation of vibration isolation platform, which will have a better guiding significance for the engineering application of such vibration isolation platform.

## 6. Conclusions

A novel 6-DOF QZS vibration isolation platform based on the leaf spring structure is proposed, and its structural characteristics and debugging methods are described. Through the static analysis in different degrees of freedom, the effects of stiffness and dimension on

the stiffness-displacement (rotation angle) relationship of the vibration isolation system are obtained. Then, the influences of the damping and dimension parameters on the stability of the system were obtained through dynamic analysis. Finally, the transmissibility characteristics were analyzed and testified to evaluate the vibration isolation performance of the essential parameters determined in the static analysis and stability analysis. Through the above analysis, the following conclusions are drawn.

- (1) Three design parameters, including  $A$ ,  $\hat{k}_3$ , and  $\hat{L}_0$ , have the greatest influence on the vibration isolation performance of the platform, in which, in order to make the stiffness of the isolation system close to zero, the value of  $A$  should be near to 1, and the values of  $\hat{k}_3$  and  $\hat{L}_0$  should be minimal under the premise of ensuring the static load capacity of the system;
- (2) The load capacity of the isolator is mainly related to the stiffness of the leaf spring and the deformation of the central spring under static load. Besides, in order to ensure that the stiffness of the system is close to zero, the stiffness of the suspension spring and the central spring should be as similar as possible.
- (3) The system will tend to be more stable and there will be a better vibration isolation effect when the damping and length parameters increase. Besides, the bifurcation of the isolation system will be caused as the amplitude of the excitation force increases, so that the vibration isolation effect will also decrease. The reason for that is the compressing length of the leaf spring and suspension spring will decrease, and there is not any variant in the central spring. Hence, increasing the slant length will improve the vibration isolation effect, nevertheless the unstable response will also be introduced.
- (4) There is a jumping phenomenon in the QZS vibration isolation platform, and its jumping interval are 0.32 Hz (vertical) and 0.31 Hz (horizontal). Through the experiment, the cause of the jump phenomenon is caused by the inconsistency between the jump frequency and the jump frequency generated in the forward and reverse frequency sweep.

At present, it is still innovative to use quasi-zero stiffness vibration isolation technology to solve the problem of low frequency and high efficiency vibration isolation. In the future, relevant research should focus on its engineering realizability and reliability, for example, the system damping changes caused by the difference in lubrication degree and tightness degree of the leaf spring and other core components in the process of production and installation, as well as the impact of the fastness changes in the process of long-term use. All of these problems need to be analyzed theoretically and studied regularly.

**Author Contributions:** Conceptualization, Z.W. and C.H.; methodology, Y.X.; software, D.L.; validation, Z.W., C.H., and Y.X.; formal analysis, Y.X.; investigation, Z.L.; resources, Z.W.; data curation, Y.X.; writing—original draft preparation, Y.X.; writing—review and editing, L.K.; visualization, C.H.; supervision, Z.W.; project administration, D.L.; funding acquisition, W.D. All authors have read and agreed to the published version of the manuscript.

**Funding:** This research was funded by the Shandong Provincial Natural Science Foundation, China, grant number ZR2021MD106, ZR2020QA045, and Qingdao Independent Innovation Major Project, grant number 21-1-2-2-hy.

**Institutional Review Board Statement:** Not applicable.

**Informed Consent Statement:** Not applicable.

**Data Availability Statement:** Data are contained within the article.

**Conflicts of Interest:** The authors declare no conflict of interest. The funders had no role in the design of the study; in the collection, analyses, or interpretation of data; in the writing of the manuscript, or in the decision to publish the results.

**Nomenclature**

| Parameters  | Symbol               | Parameters  | Symbol               |
|---|----------------------|---|----------------------|
| Ratio of $k_1$ and $k_2$                                      | $A$                  | Length of suspension spring in horizontal displacement              | $L_{2h1}, L_{2h2}$   |
| Width of the leaf spring                                      | $b$                  | Length of suspension spring in horizontal rotation                  | $L_{2hm1}, L_{2hm2}$ |
| Damping   | $C_i$                | Length of suspension spring in vertical displacement                | $L_{2v}$             |
| Elasticity modulus  | $E$                  | Bearing capacity of the platform                                    | $m$                  |
| Lord force  | $F$                  | Torque around the vertical axis                                     | $M_{vm}$             |
| Tensile force provided by the central spring                  | $F_1$                | Torque around the horizontal axis                                   | $M_{hm}$             |
| Tensile force provided by the suspension spring               | $F_2$                | Transmissibility  | $T_i$                |
| Vertical force  | $F_{vd}$             | Vertical displacement of the isolator bearing the static load force | $x_0$                |
| Horizontal force  | $F_{hd}$             | Downward displacement of the top plate                              | $x_1$                |
| Elastic force of suspension spring in vertical displacement   | $F_{2v}$             | Leftward displacement of the top plate                              | $x_2$                |
| Elastic force of suspension spring in horizontal displacement | $F_{2h1}, F_{2h2}$   |   |                      |
| Elastic force of suspension spring in vertical rotation       | $F_{2vm}$            | <i>Greek letters</i>  |                      |
| Elastic force of suspension spring in horizontal rotation     | $F_{2hm1}, F_{2hm2}$ | Rotation angle of the leaf spring                                   | $\alpha, \beta$      |
| Elastic force of leaf spring in vertical displacement         | $F_{3v}$             | Product of $\omega_0$ and $t$                                       | $\tau$               |
| Elastic force of leaf spring in vertical rotation             | $F_{3vm}$            | Damping ratio   | $\zeta_i$            |
| Elastic force of leaf spring in horizontal rotation           | $F_{3hm}$            | Rotation angle of the leaf spring in vertical displacement          | $\theta_v$           |
| Acceleration of gravity                                       | $g$                  | Rotation angle of the leaf spring in horizontal displacement        | $\theta_h$           |
| Amplitude of excitation force                                 | $H_{1,2,3,4}$        | Rotation angle of the leaf spring in vertical rotation              | $\theta_{vm}$        |
| Stiffness of central spring                                   | $k_1$                | Rotation angle of the leaf spring in horizontal rotation            | $\theta_{hm}$        |
| Stiffness of suspension spring                                | $k_2$                |   |                      |
| Stiffness of leaf spring                                      | $k_3$                | <i>Superscripts</i>   |                      |
| Stiffness in vertical displacement                            | $k_{vd}$             | Denotes dimensionless quantity                                      | $\hat{\quad}$        |
| Initial stretch length of the central spring                  | $L_1$                |   |                      |
| Radius of top plate   | $L_0$                |   |                      |
| Unstretched length of the suspension spring                   | $L_{20}$             |   |                      |

## References

1. Rivin, E. Passive vibration isolation. *Appl. Mech. Rev.* **2003**, *57*, 31–32. [[CrossRef](#)]
2. Ibrahim, R.A. Recent advances in nonlinear passive vibration isolators. *J. Sound Vib.* **2008**, *314*, 371–452. [[CrossRef](#)]
3. Alabuzhev, P.M.; Rivin, E.I. *Vibration Protecting and Measuring Systems with Quasi-Zero Stiffness*; Hemisphere Publishing Corporation: New York, NY, USA, 1989; pp. 55–78.
4. Platus, D.L. Negative-stiffness-mechanism vibration isolation systems. *Proc. SPIE Int. Soc. Opt. Eng.* **1999**, *3786*, 44–54.
5. Liu, X.; Huang, X.; Hua, H. On the characteristics of a quasi-zero stiffness isolator using Euler buckled beam as negative stiffness corrector. *J. Sound Vib.* **2013**, *332*, 3359–3376. [[CrossRef](#)]
6. Kovacic, I.; Brennan, M.J.; Waters, T.P. A study of a nonlinear vibration isolator with a quasi-zero stiffness characteristic. *J. Sound Vib.* **2008**, *315*, 700–711. [[CrossRef](#)]
7. Meng, Q.; Yang, X.; Li, W.; Lu, E.; Sheng, L. Research and analysis of quasi-zero-stiffness isolator with geometric nonlinear damping. *Shock Vib.* **2017**, *2017*, 6719054. [[CrossRef](#)]
8. Carrella, A.; Brennan, M.J.; Waters, T.P.; Shin, K. On the design of a high-static-low-dynamic stiffness isolator using linear mechanical springs and magnets. *J. Sound Vib.* **2008**, *315*, 712–720. [[CrossRef](#)]
9. Shin, K. On the performance of a single degree-of-freedom high-static-low-dynamic stiffness magnetic vibration isolator. *Int. J. Precis. Eng. Manuf.* **2014**, *15*, 439–445. [[CrossRef](#)]
10. Shan, Y.; Wu, W.; Chen, X. Design of a miniaturized pneumatic vibration isolator with high-static-low-dynamic stiffness. *J. Vib. Acoust.* **2015**, *137*, 045001. [[CrossRef](#)]
11. Robertson, W.S.; Kidner, M.R.F.; Cazzolato, B.S.; Zander, A.C. Theoretical design parameters for a quasi-zero stiffness magnetic spring for vibration isolation. *J. Sound Vib.* **2009**, *326*, 88–103. [[CrossRef](#)]
12. Yoshikazu, A.; Kosuke, K.; Takehiko, A.; Takeshi, M.; Toshihiro, O.; Ryosuke, K. Integrated mechanical and material design of quasi-zero-stiffness vibration isolator with superelastic Cu-Al-Mn shape memory alloy bars. *J. Sound Vib.* **2015**, *358*, 74–83.
13. Dai, H.; Jing, X.; Wang, Y.; Yue, X.; Yuan, J. Post-capture vibration suppression of spacecraft via a bio-inspired isolation system. *Mech. Syst. Signal Process.* **2018**, *105*, 214–240. [[CrossRef](#)]
14. Wu, Z.; Jing, X.; Bian, J.; Li, F.; Allen, R. Vibration isolation by exploring bio-inspired structural nonlinearity. *Bioinspir. Biomim.* **2015**, *10*, 056015. [[CrossRef](#)]
15. Gatti, G. A k-shaped spring configuration to boost elastic potential energy. *Smart Mater. Struct.* **2019**, *28*, 077002. [[CrossRef](#)]
16. Gatti, G. Statics and dynamics of a nonlinear oscillator with quasi-zero stiffness behaviour for large deflections. *Commun. Nonlinear Sci.* **2020**, *83*, 105143. [[CrossRef](#)]
17. Kim, G.W.; Kang, J. The V-shaped band-stop vibration isolator inspired by middle ear. *Appl. Acoust.* **2019**, *150*, 162–168. [[CrossRef](#)]
18. Wu, Z.; Jing, X.; Sun, B.; Li, F. A 6DOF passive vibration isolator using x-shape supporting structures. *J. Sound Vib.* **2016**, *380*, 90–111. [[CrossRef](#)]
19. Zhou, J.; Xiao, Q.; Xu, D.; Ouyang, H.; Li, Y. A novel quasi-zero-stiffness strut and its applications in six-degree-of-freedom vibration isolation platform. *J. Sound Vib.* **2017**, *394*, 59–74. [[CrossRef](#)]
20. Wang, Y.; Liu, H. Six degree-of-freedom microvibration hybrid control system for high technology facilities. *J. Struct. Stab. Dyn.* **2009**, *9*, 437–460. [[CrossRef](#)]
21. Zhang, Y.; Chen, Z.; Jiao, Y. A hybrid vibration isolator: Design, control, and experiments. *Proc. Inst. Mech. Eng. Part C J. Mech. Eng. Sci.* **2016**, *230*, 2982–2995. [[CrossRef](#)]
22. Touze, C.; Vizzaccaro, A.; Thomas, O. Model order reduction methods for geometrically nonlinear structures: A review of nonlinear techniques. *Nonlinear Dyn.* **2021**, *105*, 1141–1190. [[CrossRef](#)]